

Lepto-philic 2-HDM + singlet scalar portal induced fermionic dark matter

Sukanta Dutta,^{a,†} Ashok Goyal,^{b,#} Manvinder Pal Singh,^{a,b,\$}

^a*SGTB Khalsa College, University of Delhi, Delhi, India.*

^b*Department of Physics & Astrophysics, University of Delhi, Delhi, India.*

E-mail: †Sukanta.Dutta@gmail.com, #agoyal45@yahoo.com, [\\$](mailto:$)

Corresponding Author: manvinderpal666@yahoo.com

ABSTRACT: We explore the possibility that the discrepancy in the observed anomalous magnetic moment of the muon Δa_μ and the predicted relic abundance of Dark Matter by Planck data, can be explained in a lepto-philic 2-HDM augmented by a real SM singlet scalar of mass ~ 10 -80 GeV. We constrain the model from the observed Higgs Decay width at LHC, LEP searches for low mass exotic scalars and anomalous magnetic moment of an electron Δa_e . This constrained light singlet scalar serves as a portal for the fermionic Dark Matter, which contributes to the required relic density of the universe. The model is found to be consistent with the present observations from the Direct and Indirect DM detection experiments.

Contents

1	Introduction	1
2	The Model	2
3	Electro-Weak Constraints	5
3.1	Anomalous Magnetic Moment of Muon	5
3.2	LEP and Δa_e Constraints	8
3.3	Constraints from Higgs decay-width	8
4	Dark matter Phenomenology	11
4.1	Computation of the Relic Density	11
4.2	Direct Detection	13
4.3	Indirect detection	14
5	Summary	15
A	Model Parameters	17
B	Decay widths of the singlet scalar S^0	17
C	Thermally averaged scattering cross-sections	18
D	Triple scalar coupling	19

1 Introduction

Investigations into the nature of dark matter (DM) particles and their interactions is an important field of research in Astro-particle physics. The Atlas and CMS collaborations [1, 2] at the Large Hadron Collider (LHC) are searching for the signature of DM particles involving missing energy (\cancel{E}_T) accompanied by a single or two jet events. Direct detection experiments measure the nuclear-recoil energy and its spectrum in DM-Nucleon elastic scattering [3, 4]. In addition, there are Indirect detection experiment [5] searching for the DM annihilation into photons and neutrinos in cosmic rays. These experiments have now reached a level of sensitivity where a significant part of parameter space required for the observed relic density, if contributed by the dark matter composed of Weakly interacting massive particles (WIMPs) that survive as thermal relics, has been excluded. The null results of these direct and indirect experiments have given rise to the consideration of ideas where the dark matter is restricted to couple exclusively to either Standard Model (SM) leptons (lepto-philic) or only to top quarks (top-philic). In these scenarios the DM-Nucleon scattering occurs only at the loop level and the constraints from direct detection are weaker.

Recently a simplified *Dark Higgs portal model* of the order of \lesssim few GeV, that couples predominantly to leptons with the coupling constant $\sim m_l/v_o$ where m_l is the lepton mass and v_o is the Higgs VEV, has been considered in the literature [6]. This model induces large contribution to the anomalous magnetic moment of muon and can explain the existing discrepancy between the experimental observation $a_\mu^{\text{exp}} = 11\,659\,209.1(5.4)(3.3) \times 10^{-10}$ [7] and theoretical prediction $a_\mu^{\text{SM}} = 116\,591\,823(1)(34)(26) \times 10^{-11}$ [7, 8] of the muon anomalous magnetic moment $\Delta a_\mu \equiv a_\mu^{\text{exp}} - a_\mu^{\text{SM}} = 268(63) \times 10^{-11}$ [7] without compromising the experimental measurement of electron anomalous magnetic moment $a_e^{\text{exp}} = (1159.65218091 \pm 0.00000026) \times 10^{-6}$ [9]. It has been shown in the literature [10], that with the inclusion of an additional singlet scalar below the electro-weak scale to the lepto-philic 2-HDM makes the model UV complete. This UV complete model with an extra singlet scalar $\sim < 10$ GeV successfully explains the existing 3σ discrepancy of muon anomalous magnetic moment and is consistent with the constraints on the model parameters from muon and meson decays [11–14]. These results have been analyzed for $0.01 \text{ GeV} < m_{S^0} < 10 \text{ GeV}$ when compared with those for the singlet neutral vector Z' searches at B factories such as BaBar [15], from electron beam dump experiments [16] and electroweak precision experiments [17] etc.

In reference [18], the authors have explored the possibility of explaining the anomalous magnetic moment of muon with an additional lepto-philic light scalar mediator assuming the *universal coupling* of the scalar with all leptons constrained from the LEP [19] resonant production and the BaBar experiments [15]. These constraints were found to exclude all of the scalar mediator mass range except between 10 MeV and 300 MeV.

In the current paper we consider fermionic dark matter that couples predominately with SM leptons through the *non-universal* couplings with the *scalar portal* in the UV complete lepto-philic 2-HDM model. We relax the requirement of the very light scalar considered in [10] and investigate parameter space for a comparatively heavier scalar $10 \text{ GeV} \lesssim m_{S^0} \lesssim 80 \text{ GeV}$. In section 2, we give a brief review of this simplified model, using the full Lagrangian and couplings of the Singlet scalar S^0 with all model particles. In section 3, we calculate the contribution from scalars (S^0, H^0, A^0, H^\pm) to the anomalous magnetic moment of the muon and discuss bounds on the model parameters from LEP-II, Δa_e and upper bound on the observed total Higgs decay width. In section 4, we further restrict the parameter space from the observed relic density, direct and indirect experimental data by keeping the parameters consistent with observed value of the Δa_μ . Section 5 is devoted to discussion and summary of results.

2 The Model

We consider a UV complete lepton specific 2-HDM with a singlet *scalar portal* interacting with the fermionic DM. In this model the two Higgs doublets Φ_1 and Φ_2 so arranged that Φ_1 couples exclusively to leptons while Φ_2 couples exclusively to quarks. The ratio of their VEV's $\langle \Phi_1 \rangle / \langle \Phi_2 \rangle \equiv v_2 / v_1 = \tan \beta$ is assumed to be large. In this model the scalars (other than that identified with the CP even $h^0 \sim 125 \text{ GeV}$) couple to leptons with coupling enhanced by $\tan \beta$. A mixing term in the potential $A_{12} [\Phi_1^\dagger \Phi_2 + \Phi_2^\dagger \Phi_1] \varphi^0$ results in the

physical scalar S^0 coupling to leptons with strength proportional to m_l/v_o where

$$v_o \equiv \sqrt{v_1^2 + v_2^2} = 246 \text{ GeV}. \quad (2.1)$$

The full scalar potential is given by

$$V(\Phi_1, \Phi_2, \varphi^0) = V_{2-HDM} + V_{\varphi^0} + V_{\text{portal}} \quad (2.2)$$

where CP conserving V_{2-HDM} is given as

$$\begin{aligned} V_{2-HDM}(\Phi_1, \Phi_2) = & m_{11}^2 \Phi_1^\dagger \Phi_1 + m_{22}^2 \Phi_2^\dagger \Phi_2 - (m_{12}^2 \Phi_1^\dagger \Phi_2 + \text{h.c.}) + \frac{\lambda_1}{2} (\Phi_1^\dagger \Phi_1)^2 + \frac{\lambda_2}{2} (\Phi_2^\dagger \Phi_2)^2 \\ & + \lambda_3 (\Phi_1^\dagger \Phi_1) (\Phi_2^\dagger \Phi_2) + \lambda_4 (\Phi_1^\dagger \Phi_2) (\Phi_2^\dagger \Phi_1) + \left\{ \frac{\lambda_5}{2} (\Phi_1^\dagger \Phi_2)^2 + \text{h.c.} \right\} \end{aligned} \quad (2.3)$$

and V_{φ^0} and V_{portal} is assumed to be

$$V_{\varphi^0} = B\varphi^0 + \frac{1}{2}m_0^2(\varphi^0)^2 + \frac{A_{\varphi^0}}{2}(\varphi^0)^3 + \frac{\lambda_{\varphi^0}}{4}(\varphi^0)^4. \quad (2.4)$$

$$V_{\text{portal}} = A_{11} (\Phi_1^\dagger \Phi_1) \varphi^0 + A_{12} (\Phi_1^\dagger \Phi_2 + \Phi_2^\dagger \Phi_1) \varphi^0 + A_{22} (\Phi_2^\dagger \Phi_2) \varphi^0. \quad (2.5)$$

where the scalar doublets

$$\Phi_1 = \frac{1}{\sqrt{2}} \begin{pmatrix} \sqrt{2}\omega_1^+ \\ (\rho_1 + v_o \cos \beta) + iz_1 \end{pmatrix}; \quad \Phi_2 = \frac{1}{\sqrt{2}} \begin{pmatrix} \sqrt{2}\omega_2^+ \\ \rho_2 + v_o \sin \beta + iz_2 \end{pmatrix}. \quad (2.6)$$

are written in terms of the mass eigenstates G^0 , A^0 , G^\pm and H^\mp as

$$\begin{pmatrix} z_1 \\ z_2 \end{pmatrix} = \begin{pmatrix} \cos \beta & -\sin \beta \\ \sin \beta & \cos \beta \end{pmatrix} \begin{pmatrix} G^0 \\ A^0 \end{pmatrix}; \quad \begin{pmatrix} \omega_1 \\ \omega_2 \end{pmatrix} = \begin{pmatrix} \cos \beta & -\sin \beta \\ \sin \beta & \cos \beta \end{pmatrix} \begin{pmatrix} G^\pm \\ H^\pm \end{pmatrix}. \quad (2.7)$$

Here G^0 & G^\pm are Nambu-Goldstone Bosons absorbed by the Z^0 and W^\pm vector Bosons, A^0 is the pseudo-scalar and H^\pm are the charged Higgs. The neutral scalar states too are written in terms of mass eigen-states and in the perturbation limit are given by.

$$\begin{pmatrix} \rho_1 \\ \rho_2 \\ \varphi^0 \end{pmatrix} \simeq \begin{pmatrix} -\sin \alpha & \cos \alpha & \delta_{13} \\ \cos \alpha & \sin \alpha & \delta_{23} \\ \delta_{31} & \delta_{32} & 1 \end{pmatrix} \begin{pmatrix} h^0 \\ H^0 \\ S^0 \end{pmatrix}; \quad (2.8)$$

The additional mixing angles δ_{13} and δ_{23} are given as

$$\delta_{13} \simeq -\frac{v_0 A_{12}}{m_{H^0}^2}, \quad \delta_{23} \simeq -\frac{v_0 A_{12}}{m_{h^0}^2} \left[1 + \xi_\ell^{h^0} \left(1 - \frac{m_{h^0}^2}{m_{H^0}^2} \right) \right] \cot \beta, \quad (2.9)$$

This configuration of mixing matrix holds for small δ_{13} , δ_{23} , such that $\sin \delta_{13} \simeq \delta_{13}$, $\sin \delta_{23} \simeq \delta_{23}$ and $\xi_\ell^{h^0}$ is chosen to be ~ 1 in the alignment *i.e.* $(\beta - \alpha) \simeq \pi/2$.

ξ_ψ^ϕ/ξ_V^ϕ	S^0	h^0	H^0	A^0	H^\pm
ℓ	δ_{13}/c_β	$-s_\alpha/c_\beta$	c_α/c_β	$-s_\beta/c_\beta$	$-s_\beta/c_\beta$
u_q	δ_{23}/s_β	c_α/s_β	s_α/s_β	c_β/s_β	c_β/s_β
d_q	δ_{23}/s_β	c_α/s_β	s_α/s_β	$-c_\beta/s_\beta$	c_β/s_β
Z^0/W^\pm	$\delta_{13}c_\beta + \delta_{23}s_\beta$	$s_{(\beta-\alpha)}$	$c_{(\beta-\alpha)}$	-	-

Table 1: Values of ξ_ψ^ϕ and ξ_V^ϕ for $\phi = S^0, h^0, H^0, A^0$ and H^\pm ; $\psi = \ell, u_q$ and d_q ; $V = W^\pm$ and Z^0 in the leptophilic 2-HDM+S⁰ model. These values coincide with couplings given in reference [10] in the alignment limit *i.e.* $(\beta - \alpha) \simeq \pi/2$. In the table s and c stands for \sin and \cos respectively.

The spectrum of the model at the electro-weak scale is dominated by V_{2-HDM} . The V_{φ^0} and V_{portal} interactions are treated as perturbations. After diagonalization of the scalar mass matrix, the masses of the physical neutral scalars are given by

$$m_{S^0}^2 \simeq m_0^2 + \delta_{13} M_{13}^2 + \delta_{23} M_{23}^2 \quad (2.10)$$

$$m_{h^0, H^0}^2 \simeq \frac{1}{2} \left[M_{11}^2 + M_{22}^2 \mp \sqrt{(M_{11}^2 - M_{22}^2)^2 + 4 M_{12}^4} \right] \quad (2.11)$$

where

$$\begin{aligned} M_{11}^2 &= m_{12}^2 \tan \beta + \lambda_1 v_0^2 \cos^2 \beta; & M_{12}^2 &= -m_{12}^2 + (\lambda_3 + \lambda_4 + \lambda_5) v_0^2 \cos \beta \sin \beta; \\ M_{22}^2 &= m_{22}^2 \cot \beta + \lambda_2 v_0^2 \sin^2 \beta; & M_{13}^2 &= v_0 A_{12} \sin \beta; & M_{23}^2 &= v_0 A_{12} \cos \beta; \end{aligned} \quad (2.12)$$

In the alignment limit, one of the neutral CP even scalar $h^0 \approx 125$ GeV is identified with the SM Higgs.

The coefficients $m_0^2, m_{11}^2, m_{22}^2$ and λ_i for $i = 1, \dots, 5$ are explicitly defined in terms of the physical scalar masses, mixing angles α and β and the free parameter m_{12}^2 and are given in the Appendix A. Terms associated with A_{11} are proportional to $\cot \beta$ and therefore can be neglected as they are highly suppressed in the large $\tan \beta$ limit. Terms proportional to A_{22} are tightly constrained from the existing data at LHC on decay of a heavy exotic scalar to di-higgs channel and therefore they are dropped. The coefficient B is fixed by redefinition of the field φ^0 to avoid a non-zero VEV for itself.

The Yukawa couplings arising due Higgs Doublets Φ_1 and Φ_2 in type-X 2-HDM is given by

$$-\mathcal{L}_Y = \bar{L} Y_e \Phi_1 e_R + \bar{Q} Y_d \Phi_2 d_R + \bar{Q} Y_u \tilde{\Phi}_2 u_R + \text{h.c.}, \quad (2.13)$$

$$m_e = \cos \beta \times \frac{Y_e v_o}{\sqrt{2}}, \quad m_{u(d)} = \sin \beta \times \frac{Y_{u(d)} v_o}{\sqrt{2}}. \quad (2.14)$$

We re-write the Yukawa interactions of the physical neutral states as

$$-\mathcal{L}_Y \supset \sum_{\phi=S^0, h^0, H^0} \sum_{\psi=\ell, q} \xi_\psi^\phi \frac{m_\psi}{v_o} \phi \bar{\psi} \psi \quad (2.15)$$

The couplings ξ_ψ^ϕ are given in the first three rows of table 1. It is important to mention here that the Yukawa couplings are proportional to the fermion mass *i.e.* *non-universal* unlike

the consideration in reference [18]. We also observe that in the large $\tan\beta$ limit regime, the Yukawa couplings due to additional neutral scalars H^0 & S^0 in the lepton and quark sectors are enhanced and suppressed by $\tan\beta$ respectively.

The interaction of the neutral scalar mass eigenstates with the weak gauge Bosons are given by

$$\mathcal{L} \supset \sum_{\phi \equiv S^0, h^0, H^0} \frac{\phi}{v_o} \left(2 \xi_{W^\pm}^\phi m_{W^\pm}^2 W_\mu^+ W^{-\mu} + \xi_{Z^0}^\phi m_{Z^0}^2 Z_\mu^0 Z^{0\mu} \right). \quad (2.16)$$

The couplings ξ_V^ϕ are given in the last row of table 1. It is to be noted that for $m_{H^0} \gg m_{h^0}$, the singlet scalar coupling with Z^0 Boson can be fairly approximated as $\simeq \delta_{23} \sin\beta$.

The triple scalar couplings of the mass eigen states are given in the Appendix D, some of which can be constrained from the observed Higgs decay width and exotic scalar Boson searches at LEP, TeVatron and LHC.

3 Electro-Weak Constraints

3.1 Anomalous Magnetic Moment of Muon

We begin our analysis by evaluating the parameter space allowed from 3σ discrepancy $a_{\mu^-}^{\text{exp}} - a_{\mu^-}^{\text{SM}} \equiv \Delta a_\mu = 268(63) \times 10^{-11}$ [7]. In lepto-philic 2-HDM + singlet *scalar portal* model all five additional scalars S^0 , H^0 , A^0 , H^\pm couple to leptons with the coupling strengths given in table 1 and thus give contributions to Δa_μ at the one-loop level and are expressed as:

$$\begin{aligned} \Delta a_\mu &= \Delta a_\mu|_{S^0} + \Delta a_\mu|_{H^0} + \Delta a_\mu|_{A^0} + \Delta a_\mu|_{H^\pm} \\ &= \frac{1}{8\pi^2} \frac{m_\mu^2}{v_o^2} \tan^2\beta \left[\delta_{13}^2 I_{S^0} + I_{H^0} + I_{A^0} + I_{H^\pm} \right]. \end{aligned} \quad (3.1)$$

Here I_i are the integrals given as

$$\begin{aligned} I_{S^0, H^0} &= \int_0^1 dz \frac{(1+z)(1-z)^2}{(1-z)^2 + z r_{S^0, H^0}^{-2}}; & I_{A^0} &= - \int_0^1 dz \frac{z^3}{r_{A^0}^{-2}(1-z) + z^2}; \text{ and} \\ I_{H^\pm} &= \int_0^1 dz \frac{z(1-z)}{(1-z) - r_{H^\pm}^{-2}} \quad \text{with } r_i \equiv \frac{m_l}{m_i} \text{ for } i \equiv S^0, H^0, A^0, H^\pm. \end{aligned} \quad (3.2)$$

We observe that in the limit $r_i \ll 1$ the charged scalar integral I_{H^\pm} is suppressed by 2-3 orders of magnitude in comparison to the other integrals for the masses of the scalars varying between 150 GeV \sim 1.6 TeV. Since the present lower bound on the charged Higgs mass from its searches at LHC is 600 GeV [20], we can neglect its contribution to the Δa_μ in our calculations.

It is also important to note that the one loop contribution from the pseudo-scalar integral I_{A^0} is opposite in sign to that of the other neutral scalars I_{H^0, h^0, S^0} , while at the level of two loops the Barr-Zee diagrams [21], it gives positive contribution to Δa_μ which may be sizable for low pseudo-scalar mass m_{A^0} because of large value of the coupling $\xi_l^{A^0}$. However, for heavy A^0 and H^0 considered here, we can safely neglect the two loop contributions.

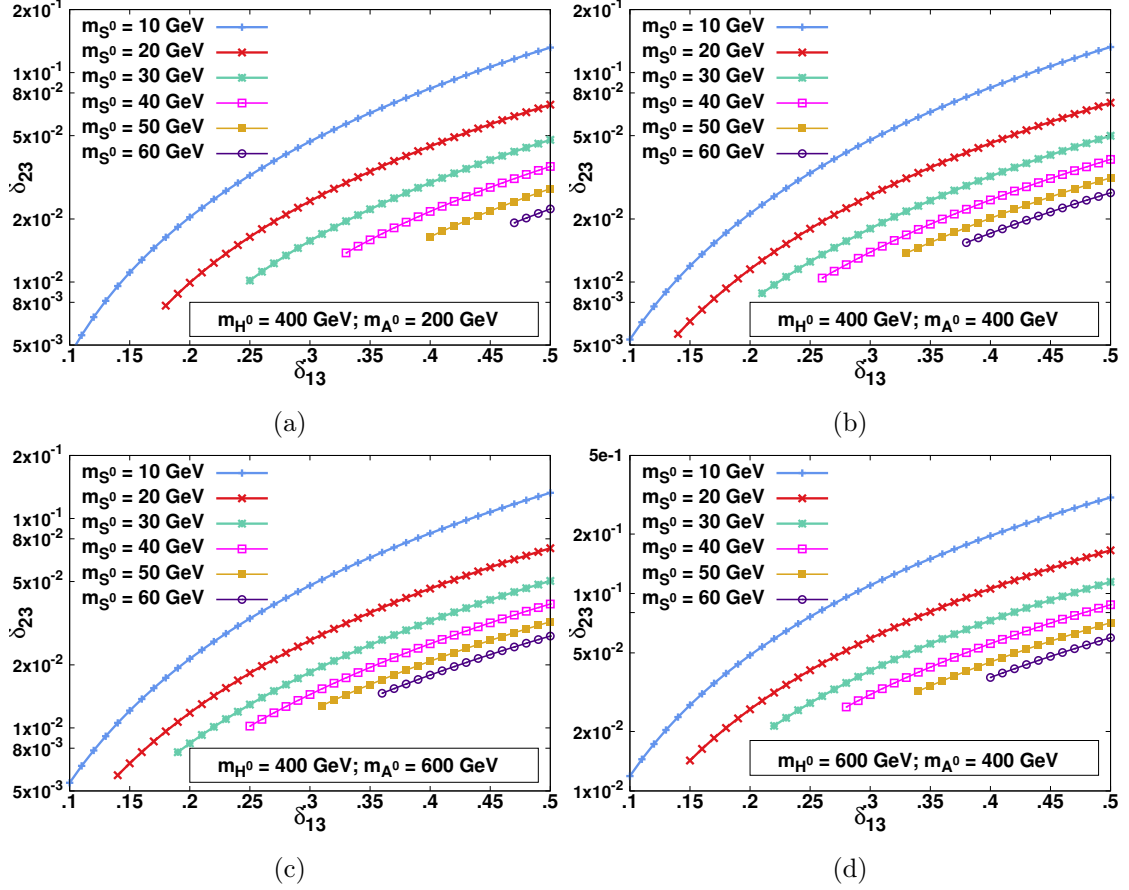


Figure 1: Figures 1a, 1b, 1c and 1d show contours on the δ_{13} - δ_{23} plane satisfying $\Delta a_\mu = 268(63) \times 10^{-11}$ corresponding to four different combinations of m_{H^0} and m_{A^0} respectively. In each panel six contours are depicted corresponding to six choices of singlet masses 10, 20, 30, 40, 50 and 60 GeV respectively.

To understand the model we study the correlation of the two mixing parameters δ_{13} and δ_{23} satisfying the Δa_μ for a given set of input masses of the physical scalars and show four correlation plots in figures 1a, 1b, 1c and 1d for varying δ_{13} . We have chosen six singlet scalar masses 10, 20, 30, 40, 50, and 60 GeV. In each panel m_{H^0} and m_{A^0} are kept fixed at values, namely (a) $m_{H^0} = 400$ GeV, $m_{A^0} = 200$ GeV, (b) $m_{H^0} = 400$ GeV, $m_{A^0} = 400$ GeV, (c) $m_{H^0} = 400$ GeV, $m_{A^0} = 600$ GeV, and (d) $m_{H^0} = 600$ GeV, $m_{A^0} = 400$ GeV. We find that relatively larger values of δ_{13} are required with the increase in scalar mass m_{S^0} . Increase in the pseudo-scalar mass m_{A^0} for fixed m_{H^0} results in the lower value of δ_{13} required to obtain the observed Δa_μ . We find that δ_{23} remains small enough for all the parameter space in order to fulfil small angle approximation.

On imposing the perturbativity constraints on the Yukawa coupling $\xi_\tau^{H^0} \equiv \tan \beta m_\tau / v_0$ involving the τ^\pm and H^0 , we compute the upper bound on the model parameter $\tan \beta \lesssim 485$. As a consequence, we observe that the values of δ_{23} also gets restricted for each variation curve exhibited in figures 1a, 1b, 1c and 1d.

The contours satisfying $\Delta a_\mu = 268(63) \times 10^{-11}$ on m_{S^0} - $\tan \beta$ plane for fixed charged

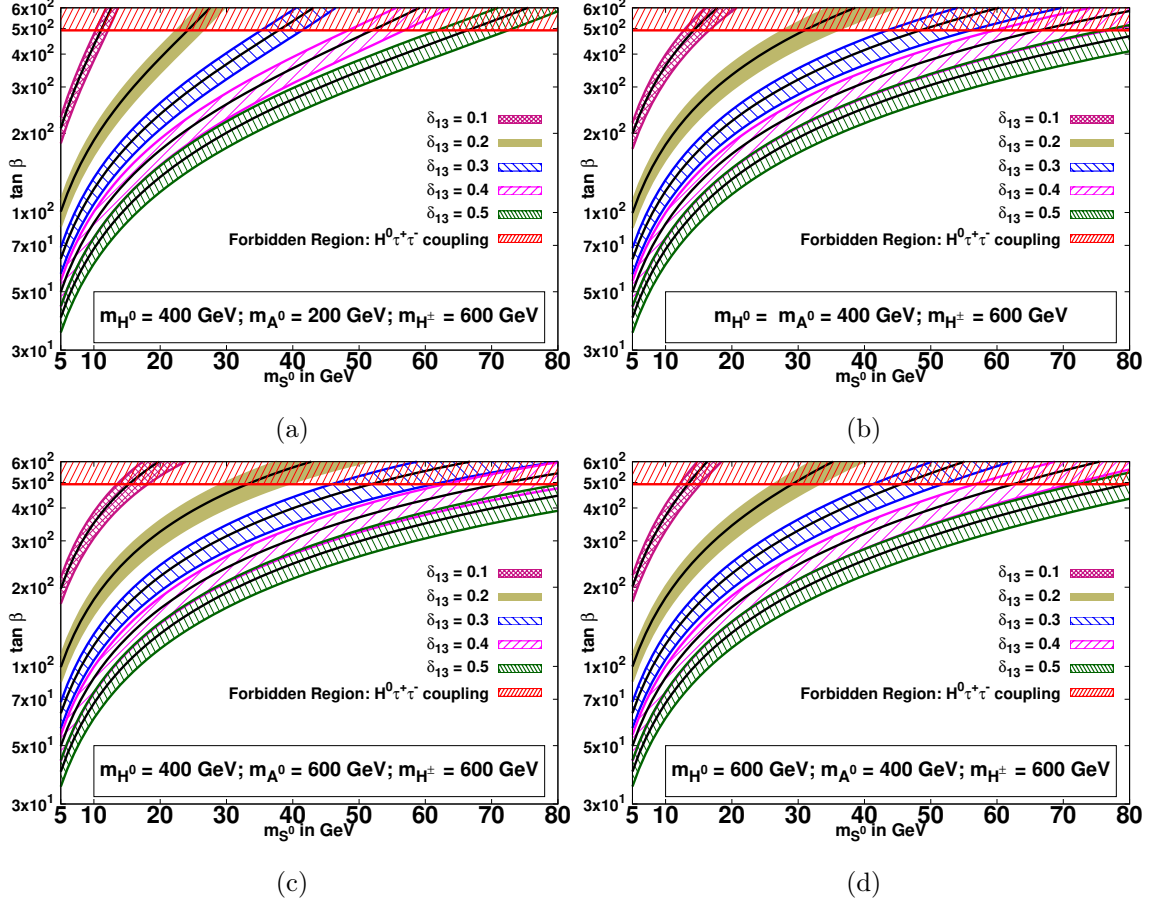


Figure 2: Figures 2a, 2b, 2c and 2d show contours on m_{S^0} - $\tan\beta$ plane satisfying $\Delta a_\mu = 268(63) \times 10^{-11}$ for fixed $m_{H^\pm} = 600$ GeV and four different combinations of m_{H^0} and m_{A^0} respectively. In each panel, five contours along-with shaded one σ bands of Δa_μ are depicted corresponding to five choices of δ_{13} 0.1, 0.2, 0.3, 0.4 and 0.5 respectively. The top horizontal band (shaded in red) in each panel shows the forbidden region on $\tan\beta$ due to the perturbative constraint on the upper limit of $H^0\tau^+\tau^-$ coupling.

Higgs mass $m_{H^\pm} = 600$ GeV are shown for four different combinations of heavy neutral Higgs mass and pseudo-scalar Higgs mass namely (a) $m_{H^0} = 400$ GeV, $m_{A^0} = 200$ GeV, (b) $m_{H^0} = 400$ GeV, $m_{A^0} = 400$ GeV, (c) $m_{H^0} = 400$ GeV, $m_{A^0} = 600$ GeV, and (d) $m_{H^0} = 600$ GeV, $m_{A^0} = 400$ GeV respectively in figures 2a, 2b, 2c and 2d. In each panel the five shaded regions, corresponding to five choices of $\delta_{13} = 0.1, 0.2, 0.3, 0.4$ and 0.5 respectively depict the 3σ allowed regions for the discrepancy in Δa_μ around its central value shown by the black lines. The horizontal band appearing at the top in all these panels shows the forbidden region on account of the perturbative constraint on the upper limit of $H^0\tau^+\tau^-$ coupling as discussed above.

As expected the allowed value of $\tan\beta$ increases with the increasing singlet scalar mass m_{S^0} and decreasing mixing angle δ_{13} . We find that a very narrow region of the singlet scalar mass is allowed by Δa_μ corresponding to $\delta_{13} \leq 0.1$.

$m_S^0(\text{GeV})$	12	15	20	25	30	35	40	45	50	55	60	65
$\xi_{Z^0}^{S^0} \lesssim$.285	.316	.398	.530	.751	1.132	1.028	.457	.260	.199	.169	.093

Table 2: Upper limits on $|\xi_{Z^0}^{S^0}|$ from bremsstrahlung process $e^+e^- \rightarrow S^0 Z^0 \rightarrow \tau^+\tau^-\tau^+\tau^-$ LEP data [22]

3.2 LEP and Δa_e Constraints

Searches for the light neutral Bosons were explored in the Higgs associated vector Boson production channels at LEP [22]. We consider the s -channel bremsstrahlung process $e^+e^- \rightarrow Z^0/\gamma^0 + h^0 \rightarrow \tau^+\tau^-\tau^+\tau^-$ whose production cross-section can be expressed in terms of the SM $h^0 Z^0$ production cross-section and given as

$$\begin{aligned} \sigma_{e^+e^- \rightarrow S^0 Z^0 \rightarrow \tau^+\tau^- Z^0} &= \sigma_{e^+e^- \rightarrow h^0 Z^0}^{\text{SM}} \times \left| \frac{\xi_{Z^0}^{S^0}}{\xi_{Z^0}^{h^0}} \right|^2 \times \text{BR}(S^0 \rightarrow \tau^+\tau^-) \\ &\equiv \sigma_{e^+e^- \rightarrow h^0 Z^0}^{\text{SM}} \times \left| \frac{\delta_{13}c_\beta + \delta_{23}s_\beta}{\sin(\beta - \alpha)} \right|^2 \times \text{BR}(S^0 \rightarrow \tau^+\tau^-). \end{aligned} \quad (3.3)$$

Since the $\text{BR}(S^0 \rightarrow \tau^+\tau^-) \simeq 1$, we can compute the exclusion limit on the upper bound on $|\xi_{Z^0}^{S^0}| \equiv |\delta_{13}c_\beta + \delta_{23}s_\beta|$ from the LEP experimental data [22], which are shown in table 2 for some chosen values of singlet scalar masses in the alignment limit.

A light neutral Vector mediator Z'^0 has also been extensively searched at LEP [19]. Vector mediator Z'^0 of mass ≤ 209 GeV is ruled out for coupling to muons $\gtrsim 0.01$ [18]. Assuming the same production cross-section corresponding to a light scalar mediator, the constraint on vector coupling can be translated to scalar coupling by multiplying a factor of $\sqrt{2}$. For the case of *non-universal* couplings where the scalar couples to the leptons with the strength proportional to its mass as is the case in our model, a further factor of $\sqrt{\frac{m_\mu}{m_e}}$ is multiplied. We therefore find the upper limit on the Yukawa coupling for leptons to be $\xi_l^{S^0} \frac{m_l}{v_0} \lesssim 0.2$.

From the constrained parameter space of the model explaining the muon Δa_μ , we find that the total contribution to anomalous magnetic moment of the electron comes out $\sim 10^{-15}$. This is two order smaller in the magnitude than the error in the measurement of $a_e \simeq \pm 2.6 \times 10^{-13}$ [9]. The present model is thus capable of accounting for the observed experimental discrepancy in the Δa_μ without transgressing the allowed Δa_e .

3.3 Constraints from Higgs decay-width

Recently a detailed analysis at a projected luminosity of 3 ab^{-1} was performed by ATLAS [23, 24] to extract the Higgs width exclusively through the four lepton channel and predicted the total Higgs decay width to be $\Gamma_{h^0} = 4.2_{-2.1}^{+1.5}$ MeV. It is important to mention that the total width of a 125 GeV SM Higgs boson is $\Gamma_H^{\text{SM}} = 4.07$ MeV, with a relative uncertainty of $\begin{matrix} +4.0\% \\ -3.9\% \end{matrix}$.

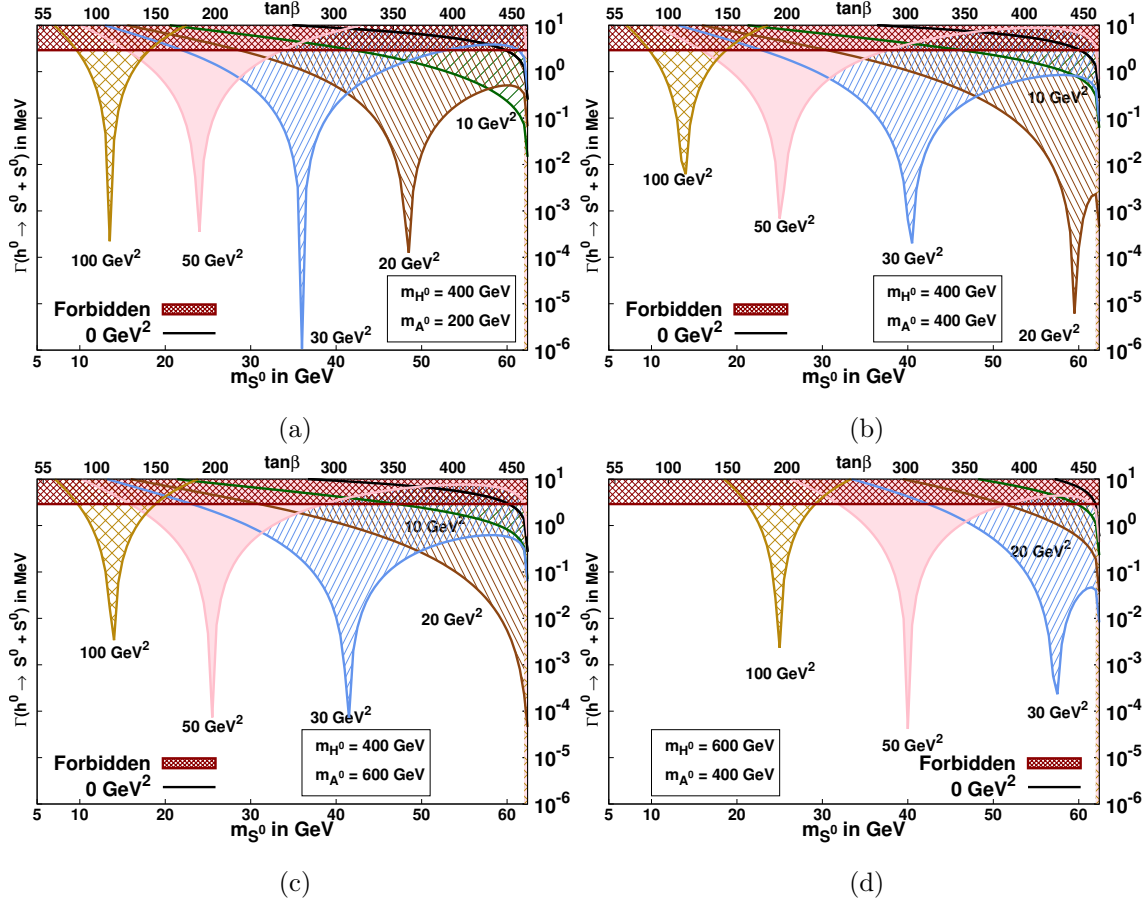


Figure 3: Figures 3a, 3b, 3c and 3d show $\Gamma_{h^0 \rightarrow S^0 S^0}$ variation with the m_{S^0} for $m_{H^\pm} = 600$ GeV, $\delta_{13} = 0.4$ and four different combinations of m_{H^0} and m_{A^0} respectively. In each panel we shade five regions corresponding to $m_{12}^2 = 10, 20, 30, 50, 100$ GeV² respectively. All points on the solid curves satisfy the discrepancy $\Delta a_\mu = 268(63) \times 10^{-11}$ and their corresponding values of $\tan\beta$ are shown in the upper x-axis of all the panels. We plot the contour corresponding to $m_{12}^2 = 0$ GeV² in black. The top horizontal band is forbidden from the measurement of the total Higgs decay width at LHC.

However, in the present model, the scalar identified with SM Higgs Boson h^0 is in addition likely to decay into two light singlet scalar portals $h^0 \rightarrow S^0 S^0$ for $m_{S^0} \leq \frac{m_{h^0}}{2}$. The partial decay width $\Gamma_{h^0 \rightarrow S^0 S^0}$ is given as

$$\Gamma_{h^0 \rightarrow S^0 S^0} = \frac{C_{h^0 S^0 S^0}^2}{32 \pi m_{h^0}} \sqrt{1 - \frac{4 m_{S^0}^2}{m_{h^0}^2}} \quad (3.4)$$

The tri-scalar coupling $C_{h^0 S^0 S^0}$ is given in equation D.1.

As total Higgs decay width is known with a fair accuracy, any contribution coming from other than SM particles should fit into the combined theoretical and experimental uncertainty. Thus, using the LHC data on total Higgs decay-width, we can put an upper limit on the tri-scalar coupling $C_{h^0 S^0 S^0}$. This upper limit is then used to constrain the parameter space of the model.

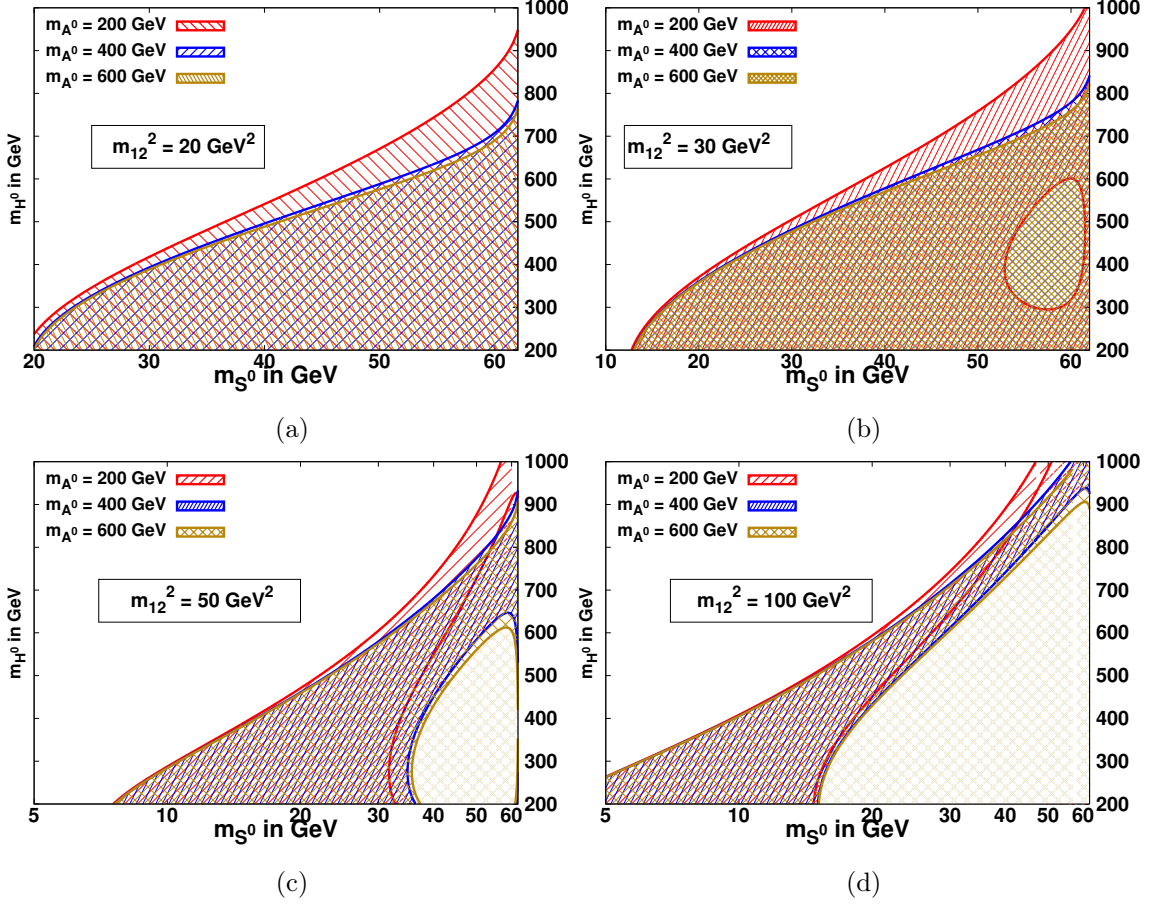


Figure 4: Figures 4a, 4b, 4c and 4d show contours on the m_{S^0} - m_{H^0} plane satisfying the upper bound on $\Gamma_{h^0 \rightarrow S^0 S^0}$ obtained from the total observed Higgs decay width $\Gamma_{h^0} = 4.2_{-2.1}^{+1.5}$ for fixed $m_{H^\pm} = 600$ GeV, $\delta_{13} = 0.4$ and four different choices of $m_{12}^2 = 20, 30, 50$ and 100 GeV². All points on the contours satisfy the discrepancy $\Delta a_\mu = 268(63) \times 10^{-11}$. Each panel has three contours corresponding to $m_{A^0} = 200, 400$ and 600 GeV respectively.

Even restricting the parameter sets to satisfy the anomalous magnetic moment and LEP observations, the model parameter m_{12}^2 remains unconstrained. However, for a given choice of δ_{13} , m_{H^0} , m_{A^0} and m_{S^0} an upper limit on $|C_{h^0 S^0 S^0}|$ constrains m_{12}^2 and thus fixes the model for further validation at colliders.

We study the partial decay-width $\Gamma_{h^0 \rightarrow S^0 S^0}$ *w.r.t.* m_{S^0} for fixed mixing angle $\delta_{13} = 0.4$ and five chosen values of the free parameter $m_{12}^2 = 10, 20, 30, 50$ and 100 GeV². We depict the variation of the partial decay width $\Gamma_{h^0 \rightarrow S^0 S^0}$ in figures 3a, 3b, 3c and 3d for four different combinations of heavy neutral Higgs and pseudo-scalar Higgs (a) $m_{H^0} = 400$ GeV and $m_{A^0} = 200$ GeV; (b) $m_{H^0} = 400$ GeV and $m_{A^0} = 400$ GeV; (c) $m_{H^0} = 400$ GeV and $m_{A^0} = 600$ GeV; and (d) $m_{H^0} = 600$ GeV and $m_{A^0} = 400$ GeV respectively. The top horizontal band in all the four panels corresponds to the forbidden region arising from the observed total Higgs decay width at LHC. We find that constraints from the total Higgs decay width further shrinks the parameter space allowed by Δa_μ between 10 GeV

$\leq m_{S^0} \leq 62 \text{ GeV}$ corresponding to $100 \text{ GeV}^2 \geq m_{12}^2 \geq 10 \text{ GeV}^2$.

To have better insight of the bearings on the model from the observed total Higgs decay width we plot the contours on the $m_{S^0} - m_{H^0}$ plane in figures 4a, 4b, 4c and 4d satisfying the upper limit on the partial decay width $\Gamma_{h^0 \rightarrow S^0 S^0}^{\text{max}}$ for four choices of m_{12}^2 respectively. In each panel, three curves depict the upper limits on the partial widths which are derived from the constraints on the total decay width from LHC corresponding to three chosen values $m_{A^0} = 200, 400$ and 600 GeV respectively. We note that with increasing m_{12}^2 the allowed dark shaded region shrinks and remains confined towards a lighter m_{S^0} .

4 Dark matter Phenomenology

We introduce a spin 1/2 fermionic dark matter particle χ which is taken to be a SM singlet with zero-hyper-charge and is odd under a discrete Z_2 symmetry. The DM χ interacts with the SM particle through the *scalar portal* S^0 . The interaction Lagrangian \mathcal{L}_{DM} is given as

$$\mathcal{L}_{DM} = i\bar{\chi}\gamma^\mu\partial_\mu\chi - m_\chi\bar{\chi}\chi + \lambda_{\chi S^0}\bar{\chi}\chi S^0 \quad (4.1)$$

We are now equipped to compute the relic density of the DM, the scattering cross-section of such DM with the nucleon and its indirect detection annihilation cross-section.

4.1 Computation of the Relic Density

In early universe, when temperature of the thermal bath was much greater than the corresponding mass of the particle species, the particles were in thermal equilibrium with the background. This equilibrium was maintained through interactions such as annihilation and scattering with other SM particles, such that the interaction rate remained greater than the expansion rate of the universe. As the Universe cooled, massive particles such as our DM candidate χ , became non-relativistic and the interaction rate with other particles became lower than the expansion rate of the universe, hence decoupling the DM and giving us the relic abundance 0.119 [25, 26] we observe today. Evolution of the number density of the DM n_χ is governed by the Boltzmann equation:

$$\frac{dn_\chi}{dt} + 3\frac{\dot{a}}{a}n_\chi = -\langle\sigma|\vec{v}|\rangle(n_\chi^2 - n_{\chi eq}^2) \quad (4.2)$$

where $\frac{\dot{a}}{a} = \sqrt{\frac{8\pi\rho}{3M_{Pl}}}$, $\langle\sigma|\vec{v}|\rangle$ is thermally averaged cross-section and

$n_{\chi eq}^2 = \mathbf{g} \left(\frac{m_\chi T}{2\pi}\right)^{\frac{3}{2}} \exp\left[\frac{-m_\chi}{T}\right]$ where \mathbf{g} is the degrees of freedom, and it is 2 for fermions. As for a massive thermal relics, freeze-out occurs when the species is non-relativistic $|\vec{v}| \ll c$. Therefore, we expand $\langle\sigma|\vec{v}|\rangle$ as $\langle\sigma|\vec{v}|\rangle = a + b|\vec{v}|^2 + \mathcal{O}(|\vec{v}|^4)$. The Boltzmann equation can be solved to give the thermal relic density [27]

$$\Omega_\chi \mathbf{h}^2 \simeq \frac{1.07 \times 10^9 x_F}{M_{Pl} \sqrt{\mathbf{g}^*(x_F)} \left(a + \frac{6b}{x_F}\right)} \quad (4.3)$$

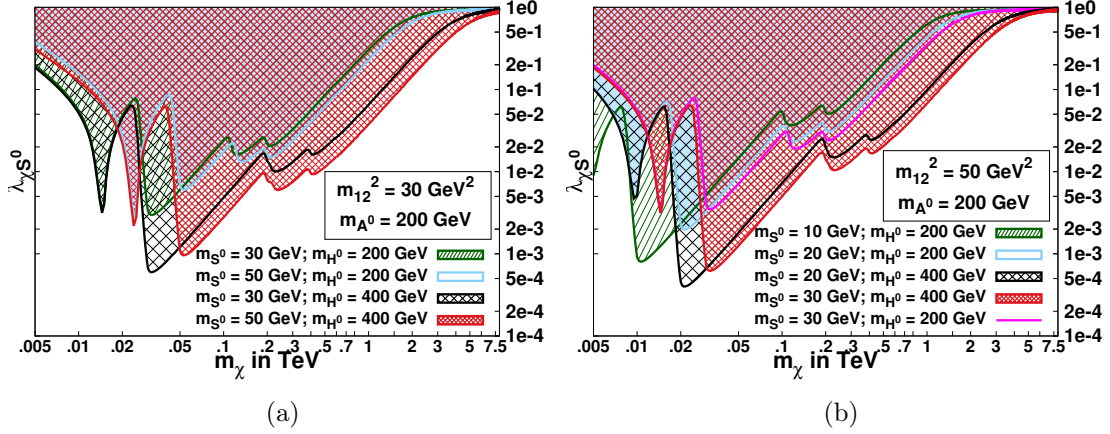


Figure 5: Figures 5a and 5b show contours on the $m_\chi - \lambda_{\chi S^0}$ plane satisfying the relic density 0.119 [25, 26] for fixed $m_{H^\pm} = 600$ GeV, $m_{A^0} = 200$ GeV, $\delta_{13} = 0.4$ and two different choices of $m_{12}^2 = 30$ and 50 GeV² respectively. All points on the contours satisfy the discrepancy $\Delta a_\mu = 268(63) \times 10^{-11}$. In the left and right panels, we show allowed (shaded) regions for four and five combinations of m_{S^0} , m_{H^0} respectively.

where \mathbf{h} is dimensionless Hubble parameter, $\mathbf{g}^*(x_F)$ is total number of dynamic degrees of freedom near freeze-out temperature T_F and $x_F = \frac{m_\chi}{T_F}$ is given by

$$x_F = \ln \left[c(c+2) \sqrt{\frac{45}{8}} \frac{\mathbf{g} M_{Pl} m_\chi \left(a + \frac{6b}{x_F} \right)}{2\pi^3 \sqrt{\mathbf{g}^*(x_F)} \sqrt{x_F}} \right] \quad (4.4)$$

where c is of the order 1. The thermal-averaged scattering cross-sections as a function of DM mass m_χ are given in the Appendix C.

To compute relic density numerically, we have used MadDM [28] and MadGraph [29]. We have generated the input model file required by MadGraph using FeynRules [30], which calculates all the required couplings and Feynman rules by using the full Lagrangian.

In figures 5a and 5b, we depict the contours of constant relic density 0.119 [25, 26] in $\lambda_{\chi S^0}$ (DM coupling) and m_χ (DM mass) plane for fixed charged Higgs mass of 600 GeV, Pseudo-scalar mass of 200 GeV and mixing angle δ_{13} , corresponding to $m_{12}^2 = 30$ and 50 GeV² respectively. The un-shaded parameter regions of DM are not allowed as they are going to over-close the universe. We observe the successive dips in the relic density contours as the additional DM annihilation channel opens up to contribute to the relic density with the increasing DM mass. Initial dip is caused by s -channel propagator. Dip observed around 0.2 TeV and 0.4 TeV are caused by opening of $\bar{\chi}\chi \rightarrow S^0 H^0$ and $\bar{\chi}\chi \rightarrow H^0 H^0$ ($A^0 A^0$) channels. In the left panel we show the allowed (shaded) regions for m_{S^0} 30 GeV and 50 GeV for varying m_{H^0} and in the right panel we show allowed regions for m_{S^0} 10 GeV, 20 GeV and 30 GeV for varying m_{H^0} . The parameter sets chosen for the calculation of the relic density are consistent with the observed value of Δa_μ and measured total Higgs decay width.

4.2 Direct Detection

Direct detection of DM measures the recoil generated by DM interaction with matter. For the case of lepto-philic DM, we have tree level DM-Electron interaction, where DM can scatter with electron in-elastically, leading to ionization of the atom to which it is bound or elastically, where excitation of atom is succeeded by de-excitation, releasing a photon. The DM-Nucleon scattering in this model occurs at the loop level and though suppressed by one or two powers of α_{em} multiplied by the loop factor, it vastly dominates over the DM-Electron and DM-Atom scattering [33–35].

In the lepto-philic 2-HDM + singlet scalar model considered here, the DM-Nucleon scattering arises through scalar-gluon-gluon coupling described by the effective Lagrangian.

$$\mathcal{L}_g^S = -\frac{\xi_t^{S^0} \alpha_s}{12\pi v_o} \left\{ \frac{3}{2} F_s \left(\frac{4m_t^2}{m_{S^0}^2} \right) \right\} G_{\mu\nu}^a G^{\mu\nu a} S^0 \quad (4.5)$$

where the loop integral $F_s \left(\frac{4m_t^2}{m_{S^0}^2} \right)$ is given in Appendix C. The effective DM-gluon interaction can then be described by the effective Lagrangian.

$$\mathcal{L}^{\chi\chi gg} = \frac{\alpha_s(m_{S^0})}{12\pi} \frac{\xi_t^{S^0} \lambda_{\chi S^0}}{v_o m_{S^0}^2} \left\{ \frac{3}{2} F_s \left(\frac{4m_t^2}{m_{S^0}^2} \right) \right\} \bar{\chi} \chi G_{\mu\nu}^a G^{\mu\nu a} \quad (4.6)$$

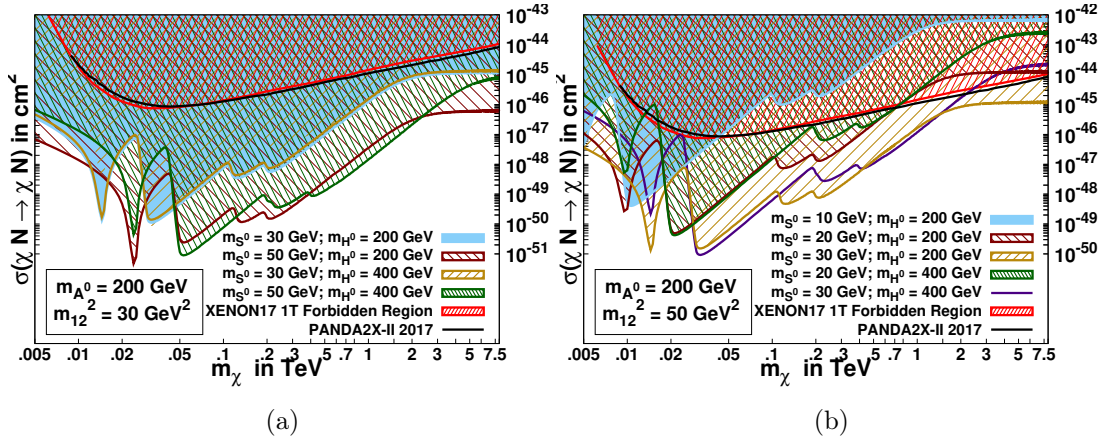


Figure 6: Figures 6a and 6b show the spin-independent DM-Nucleon cross-section variation with the m_χ for fixed $m_{H^\pm} = 600 \text{ GeV}$, $m_{A^0} = 200 \text{ GeV}$, $\delta_{13} = 0.4$ and two different choices of $m_{12}^2 = 30$ and 50 GeV^2 respectively. All points on the contours satisfy the relic density 0.119 and also explain the discrepancy $\Delta a_\mu = 268(63) \times 10^{-11}$. In the left and right panels, we plot the variation curves (bold lines) and allowed (shaded) regions for four and five combinations of m_{S^0} and m_{H^0} respectively. The upper limit from PANDA 2X-II 2017 [36] and XENON-1T [37, 38] are also shown along with the forbidden region shaded in red.

This interaction contributes to spin-independent DM-Nucleon scattering cross-section, which is given by

$$\sigma_N^{SI} = \left(\frac{2\xi_t^{S^0} \lambda_{\chi S^0} m_N}{m_{S^0}^2 27v_o} \right)^2 \frac{2}{\pi(m_\chi + m_N)^2} m_N^2 m_\chi^2$$

Using the above expression we have plotted the spin-independent DM-Nucleon scattering cross-section as a function of the the DM - singlet scalar coupling $\lambda_{\chi S^0}$ with fixed charged Higgs mass of 600 GeV, Pseudo-scalar mass of 200 GeV and mixing angle $\delta_{13} = 0.4$, corresponding to $m_{12}^2 = 30$ and 50 GeV² in figures 6a and 6b respectively. The parameter sets used to compute the Direct Detection cross-section are consistent with the observed relic density of .119 as given in figures 5a and 5b. Current bounds from spin-independent experiments like PANDA 2X-II 2017 [36] and XENON-1T [37, 38] are also shown. It can be seen that most of the parameter space for m_{S^0} less than 10 GeV is ruled out by the current bounds.

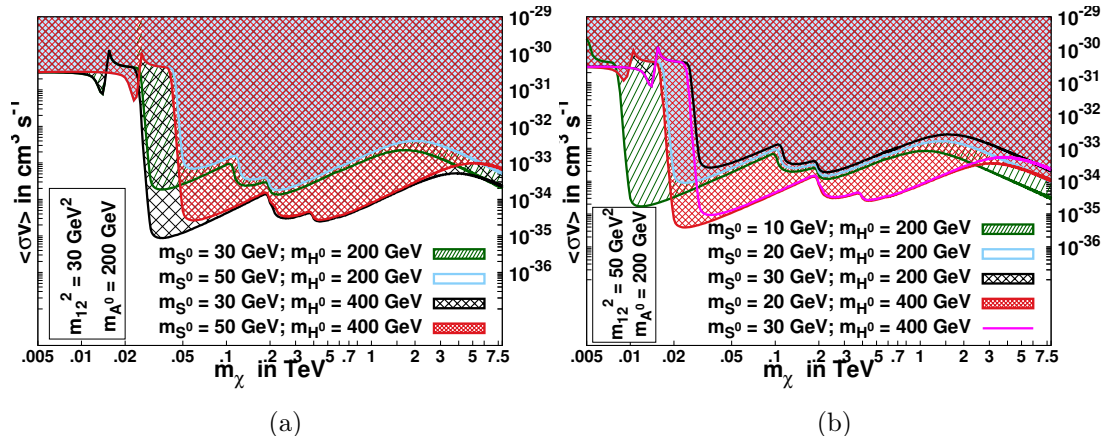


Figure 7: Figures 7a and 7b show the velocity-averaged scattering cross-section $\langle \sigma v \rangle_{\tau^+\tau^-}$ variation with the m_χ for fixed $m_{H^\pm} = 600$ GeV, $m_{A^0} = 200$ GeV, $\delta_{13} = 0.4$ and two different choices of $m_{12}^2 = 30$ and 50 GeV² respectively. All points on the contours satisfy the relic density 0.119 and also explain the discrepancy $\Delta a_\mu = 268(63) \times 10^{-11}$. In the left and right panels, we plot the variation curves (bold lines) and allowed (shaded) regions for four and five combinations of m_{S^0} and m_{H^0} respectively. The upper limit on velocity-averaged annihilation cross-section observed from Fermi-LAT, HESS etc. are at least three order of magnitude higher than the cross-section predicted by the model.

4.3 Indirect detection

Observations of diffused gamma rays from the regions of our Galaxy, such as Galactic Centre (GC) and dwarf spheroidal galaxies (dSphs), where DM density appears to be high, impose bounds on DM annihilation to SM particles. Experiments like Fermi-LAT [39, 40] and H.E.S.S. [41] have investigated DM annihilation as a possible source of the incoming photon-flux. These experiments provide us with an upper-limit to velocity-averaged scattering cross-section for various channels, which can attribute to the observed photon-flux.

In the present model, the fermionic DM can annihilate to SM particles *via* the *scalar portal* as discussed previously. As *scalar portal* coupling with leptons is enhanced by $m_l \tan \beta$, we find $\bar{\chi}\chi \rightarrow \tau^+\tau^-$ as the dominant process. The process $\bar{\chi}\chi \rightarrow \gamma\gamma$ also exists through the triangle loop in the present model and has been computed in the Appendix C, but is found to be highly suppressed.

In figures 7a and 7b we plot the velocity-averaged scattering cross-sections $\langle\sigma v\rangle(\chi\bar{\chi}\rightarrow\tau^+\tau^-)$ as a function of the the DM - *scalar portal* coupling $\lambda_{\chi S^0}$ for varying m_{S^0} , with fixed charged Higgs mass of 600 GeV, Pseudo-scalar mass of 200 GeV and mixing angle $\delta_{13} = 0.4$, corresponding to $m_{12}^2 = 30$ and 50 GeV² respectively. The parameter sets used to compute the In-direct Detection thermal averaged cross-section are consistent with the observed relic density of .119 as given in figures 5a and 5b.

We observe that the velocity averaged scattering cross-sections $\langle\sigma v\rangle(\chi\bar{\chi}\rightarrow\tau^+\tau^-)$ is *p*-wave suppressed and is, therefore, sensitive to the choice of velocity distribution of the DM in the galaxy. We find that the annihilation cross-sections are at least three orders of magnitude smaller than the current upper-limit 10^{-27} cm³/s [41] extracted from the experiments. We have used 220 Km/s (average escape velocity of galaxy) as the average velocity of the DM.

5 Summary

In this article we have made an attempt to address the observed discrepancy in anomalous magnetic moment of muon by considering a lepto-philic type **X** 2-HDM and a singlet *scalar portal* for fermionic DM. We have presented the model in such a manner where most of it's scalar sector parameters can be constrained in terms of the lower bound on the physical neutral and charged scalar's masses derived from the direct and indirect searches at LEP and LHC.

The model is analysed in the alignment limit, where one of its scalar is identified with the Higgs Boson of SM and the Yukawa couplings of fermions with the singlet scalar are found to be proportional to mass of the fermions *i.e. non-universal*. It is then validated with low energy constraints. We have illustrated the constraints from anomalous magnetic moment in figures 1 and 2 and fixed the parameters $\tan\beta$ and δ_{23} for a given δ_{13} , which is chosen to be 0.4 for our further analysis. Contrary to the results obtained in reference [18] for the singlet scalar with mass lying between 10 - 300 MeV with *universal couplings* to leptons, this study establishes the acceptability of the model to explain the discrepancy Δa_μ for singlet scalar masses lying between 10 GeV \leq 80 GeV with couplings to leptons being *non-universal*. The requirement of the Yukawa coupling $H^0\tau^+\tau^-$ to remain perturbative further imposes an upper limit $\tan\beta \leq 485$ which in turn provides the upper bound on the allowed mass range of singlet scalars to be ~ 80 GeV.

Exclusion limits on the couplings of SM gauge Bosons with the singlet scalars are obtained from the process $e^+e^- \rightarrow Z^0S^0$ at LEP-II experiment and have been displayed in table 2 for some chosen singlet scalar masses.

Validation of the model is further subjected to the observed total Higgs decay width at LHC [23, 24]. It is shown that the parameter m_{12}^2 , which has no bearing on the Δa_μ , can now be constrained from the from upper bound on the triple scalar coupling involved in the decay of SM like Higgs to a pair of singlet scalars $h^0 \rightarrow S^0S^0$. The observed total decay width of SM like Higgs h^0 restricts this additional channel and put a upper limit on the partial decay width, which has been shown in figures 3 and 4. We have found that in

the probed region of interest for singlet scalar mass, m_{12}^2 greater than 100 GeV² and less than 0 GeV² are forbidden.

We augment our analysis by including a fermionic DM candidate χ and compute the relic density which are depicted in figures 5a and 5b for $m_{12}^2 = 30$ and 50 GeV² respectively. The parameter sets chosen corresponding to points lying on contours satisfying relic density of 0.119 also fulfil the Δa_μ discrepancy and are consistent with the total Higgs decay width observed at LHC and LEP data.

The scalar portal induced DM interactions are now probed in the Direct-detection experiment by the DM-nucleon scattering propelled through the gluons. The variation of spin-independent scattering cross-sections with the DM mass are shown in figure 6 for $m_{12}^2 = 30$ and 50 GeV². It can be seen that most of the parameter space for m_{S^0} lighter than 10 GeV is excluded by current Direct-detection constraints from PANDA 2X-II and XENON-1T experiments.

The DM annihilation cross-section relevant to the space borne indirect-detection experiments, are shown in figure 7. We observe that velocity averaged scattering cross-section for the dominant channel $\bar{\chi}\chi \rightarrow \tau^+\tau^-$ is at least three orders of magnitude lower than the current reach for the DM mass varying between 5 GeV - 8 TeV.

This model with the shrunk parameter space after being constrained by low energy experiments, LEP Data, observed total decay width of Higgs at LHC and constrained by dark matter detection experiments can now be tested at the ongoing and upcoming collider searches.

Acknowledgments

Authors acknowledge the fruitful discussions with Mamta. SD and MPS acknowledge the partial financial support from the CSIR grant No. 03(1340)/15/EMR-II. MPS acknowledges the CSIR JRF fellowship for the partial financial support. SD and MPS thank IUCAA, Pune for providing the hospitality and facilities where this work was initiated.

Appendix

A Model Parameters

The parameters used in the Lagrangian for lepto-philic 2-HDM and dark matter portal singlet scalar given in equation 2.3 are expressed in terms of the physical scalar masses, mixing angles α and β and the model parameter m_{12}^2 .

$$m_0^2 = m_{S^0}^2 + \delta_{13}^2 m_{H^0}^2 [\delta_{13} \sin \beta + \delta_{23} \cos \beta] \quad (\text{A.1})$$

$$m_{11}^2 = -\frac{1}{2} [m_{H^0}^2 \cos^2 \alpha + m_{h^0}^2 \sin^2 \alpha + \{\sin \alpha \cos \alpha (m_{H^0}^2 - m_{h^0}^2) - 2 m_{12}^2\} \tan \beta] \quad (\text{A.2})$$

$$m_{22}^2 = -\frac{1}{2} [m_{h^0}^2 \cos^2 \alpha + m_{H^0}^2 \sin^2 \alpha + \{\sin \alpha \cos \alpha (m_{H^0}^2 - m_{h^0}^2) - 2 m_{12}^2\} \cot \beta] \quad (\text{A.3})$$

$$\lambda_1 = \frac{1}{v_o^2 \cos^2 \beta} [m_{H^0}^2 \cos^2 \alpha + m_{h^0}^2 \sin^2 \alpha - m_{12}^2 \tan \beta] \quad (\text{A.4})$$

$$\lambda_2 = \frac{1}{v_o^2 \sin^2 \beta} [m_{h^0}^2 \cos^2 \alpha + m_{H^0}^2 \sin^2 \alpha - m_{12}^2 \cot \beta] \quad (\text{A.5})$$

$$\lambda_3 = \frac{2}{v_o^2 \sin(2\beta)} [\sin \alpha \cos \alpha (m_{H^0}^2 - m_{h^0}^2) - m_{12}^2 + m_{H^+}^2 \sin(2\beta)] \quad (\text{A.6})$$

$$\lambda_4 = \frac{1}{v_o^2 \sin(2\beta)} [2m_{12}^2 + (m_{A^0}^2 - 2m_{H^+}^2) \sin(2\beta)] \quad (\text{A.7})$$

$$\lambda_5 = \frac{1}{v_o^2 \sin(2\beta)} [2m_{12}^2 - m_{A^0}^2 \sin(2\beta)] \quad (\text{A.8})$$

B Decay widths of the singlet scalar S^0

The tree level partial decay widths of the scalar mediator are computed and are given by:

$$\Gamma(S^0 \rightarrow f \bar{f}) = \frac{N_c}{8\pi} \left(\frac{\xi_f^S m_f}{v_o} \right)^2 m_{S^0} \left(1 - \frac{4m_f^2}{m_{S^0}^2} \right)^{3/2} \theta(m_{S^0} - 2m_f) \quad (\text{B.1})$$

where $N_c = 1$ for leptons and 3 for quarks

$$\Gamma(S^0 \rightarrow W^+ W^-) = \frac{(\xi_V^{S^0})^2}{16\pi v_o^2} m_{S^0}^3 \left(1 - \frac{4m_W^2}{m_{S^0}^2} \right)^{1/2} \left[12 \left(\frac{m_W}{m_{S^0}} \right)^4 - 4 \left(\frac{m_W}{m_{S^0}} \right)^2 + 1 \right] \times \theta(m_{S^0} - 2m_W) \quad (\text{B.2})$$

$$\Gamma(S^0 \rightarrow Z^0 Z^0) = \frac{1}{2} \Gamma(S^0 \rightarrow W^+ W^-) \text{ with } m_W \rightarrow m_Z \quad (\text{B.3})$$

$$\Gamma(S^0 \rightarrow \chi \bar{\chi}) = \frac{\lambda_{\chi S^0}^2}{8\pi} m_{S^0} \left(1 - \frac{4m_\chi^2}{m_{S^0}^2} \right)^{3/2} \theta(m_{S^0} - 2m_\chi) \quad (\text{B.4})$$

The one loop induced partial decay width of the scalar in this model arises mainly from the top quark and is given by

$$\Gamma(S^0 \rightarrow gg) = \left(\frac{m_t \xi_t^{S^0}}{V_{mSM}} \right)^2 \frac{\alpha_s^2}{72\pi^3} \frac{m_{S^0}^3}{m_t^2} \left| \frac{3}{2} F_{S^0} \left(\frac{4m_t^2}{m_{S^0}^2} \right) \right|^2 \quad (\text{B.5})$$

where $F_{S^0}(X) = X \left[1 + (1 - X) \tan^{-2} \left(\frac{1}{\sqrt{X-1}} \right) \right]$.

$$\Gamma(S^0 \rightarrow \gamma\gamma) = \frac{m_{S^0}^3}{16\pi v_0^2} \left(\frac{\alpha_{em}}{\pi} \right)^2 |I|^2 \quad (\text{B.6})$$

where I is the loop factor coming from the contribution of leptons, quarks, W^\pm boson and charged scalar(H^\pm), given by $\sum_q \xi_q^{S^0} Q_q^2 I_q + \sum_l \xi_l^{S^0} Q_l^2 I_q - \xi_{W^\pm}^{S^0} I_{W^\pm} + C_{SH+H^-} \frac{v_0}{2m_{H^\pm}^2} I_{H^\pm}$. The integrals are defined in terms of dimensionless parameter $\lambda_i = m_i^2/m_{S^0}^2$ and its function $f(\lambda)$ as

$$\begin{aligned} f(\lambda) &= -2 \left(\sin^{-1} \frac{1}{2\sqrt{\lambda}} \right), \text{ for } \lambda > \frac{1}{4} \\ &= \frac{1}{2} \left(\ln \frac{\eta^+}{\eta^-} \right)^2 - \frac{\pi^2}{2} - i\pi \frac{\eta^+}{\eta^-}, \text{ for } \lambda < \frac{1}{4} \end{aligned} \quad (\text{B.7})$$

with $\eta^\pm = \frac{1}{2} \pm \sqrt{\frac{1}{4} - \lambda}$.

The integrals are given as

$$\begin{aligned} I_q &= 3[2\lambda_q + \lambda_q(4\lambda_q - 1)f(\lambda_q)]; \quad I_l = 2\lambda_q + \lambda_q(4\lambda_q - 1)f(\lambda_q); \\ I_W &= 3\lambda_W(1 - 2\lambda_W)f(\lambda_W) - \lambda_W - \frac{1}{2}; \quad I_{H^\pm} = -\lambda_{H^\pm}[1 + 2\lambda_{H^\pm}f(H^\pm)]. \end{aligned} \quad (\text{B.8})$$

The integral I can be approximated analytically at two extreme limits and defined as

$$I \approx \sum_q \xi_q^{S^0} \frac{Q_q^2 N_c}{3} + \sum_l \xi_l^{S^0} \frac{1}{3} - \xi_{W^\pm}^{S^0} \frac{7}{4} + C_{SH+H^-} \frac{v_0}{24m_{H^\pm}^2} \quad \text{for } \lambda_i \gg 1 \quad (\text{B.9})$$

$$\approx -\frac{1}{2}\xi_{W^\pm}^{S^0} \quad \text{for } \lambda_i \ll 1 \quad (\text{B.10})$$

C Thermally averaged scattering cross-sections

We compute the thermal averaged annihilation cross-section of the fermionic DM *via* the singlet scalar portal S^0 to the SM final states. These processes contribute to the relic density of the universe and are directly used in computing the annihilation cross-section for indirect detection of the DM.

$$\langle \sigma v \rangle (\chi\bar{\chi} \rightarrow f\bar{f}) = \left(\frac{m_f \xi_f^{S^0}}{v_0} \right)^2 \lambda_{\chi S^0}^2 \frac{1}{4\pi} \left(1 - \frac{m_l^2}{m_\chi^2} \right)^{\frac{3}{2}} \frac{m_\chi^2}{(4m_\chi^2 - m_\phi^2)^2} \left(\frac{3}{x_f} \right) \theta(m_\chi - m_f) \quad (\text{C.1})$$

$$\begin{aligned} \langle \sigma v \rangle (\chi\bar{\chi} \rightarrow W^+W^-) &= \left(\frac{\xi_V^{S^0}}{v_0} \right)^2 \frac{\lambda_{\chi S^0}^2}{8\pi} \sqrt{1 - \frac{m_Z^2}{m_\chi^2}} \frac{(16m_\chi^4 + 12m_Z^4 - 16m_\chi^2 m_Z^2)}{(4m_\chi^2 - m_{S^0}^2)^2} \left(\frac{3}{x_f} \right) \\ &\times \theta(m_\chi - m_{W^\pm}) \end{aligned} \quad (\text{C.2})$$

$$\begin{aligned} \langle \sigma v \rangle (\chi\bar{\chi} \rightarrow Z^0 Z^0) &= \left(\frac{\xi_V^{S^0}}{v_0} \right)^2 \frac{\lambda_{\chi S^0}^2}{16\pi} \sqrt{1 - \frac{m_W^2}{m_\chi^2}} \frac{(16m_\chi^4 + 12m_W^4 - 16m_\chi^2 m_W^2)}{(4m_\chi^2 - m_{S^0}^2)^2} \left(\frac{3}{x_f} \right) \\ &\times \theta(m_\chi - m_{Z^0}) \end{aligned} \quad (\text{C.3})$$

$$\langle \sigma v \rangle (\chi\bar{\chi} \rightarrow gg) = \left(\frac{\xi_t^{S^0} \alpha_s \lambda_{\chi S^0}}{3\pi^{3/2} v_0} \left| \frac{3}{2} F_{S^0} \left(\frac{4m_t^2}{m_{S^0}^2} \right) \right| \right)^2 \frac{m_\chi^4}{(s - m_{S^0}^2)^2 + m_{S^0}^2 \Gamma} \left(\frac{3}{2x_f} \right) \quad (\text{C.4})$$

where $F_{S^0}(x) \equiv x \left[1 + (1-x) \tan^{-2} \frac{1}{\sqrt{x-1}} \right]$ and the cross-section arises mainly from the top quark triangle loop

$$\langle \sigma v \rangle (\chi \bar{\chi} \rightarrow \gamma \gamma) = \frac{\lambda_{\chi S^0}^2 \alpha_{em}^2}{2\pi^3 v_o^2} \frac{m_\chi^4 |I|^2}{(4m_\chi - m_{S^0}^2)^2 + m_{S^0}^2 \Gamma^2} \left(\frac{3}{x_f} \right) \quad (\text{C.5})$$

$$\begin{aligned} \langle \sigma v \rangle (\chi \bar{\chi} \rightarrow H^i H^j) &= c_0 \sum_{H^i, H^j \equiv H^0, A^0, H^\pm} C_{S^0 H^i H^j}^2 \frac{\lambda_{\chi S^0}^2}{16\pi} \lambda \left(1, \frac{m_{H^i}^2}{4m_\chi^2}, \frac{m_{H^j}^2}{4m_\chi^2} \right)^{\frac{1}{2}} \\ &\times \frac{1}{(4m_\chi^2 - m_\phi^2)^2} \left(\frac{3}{x_f} \right) \end{aligned} \quad (\text{C.6})$$

where $C_{S^0 H^i H^j}$ are the tri-linear scalar couplings given in the Appendix D; $c_0 = \frac{1}{2}$ for $i=j$ and $c_0 = 1$ for $i \neq j$; $\lambda(X, a, b) = X^2 + a^2 + b^2 - 2ab - 2aX - 2bX$.

In addition to s -channel processes considered above, we also have contributions to the relic density from t -channel process $\chi \bar{\chi} \rightarrow S^0 S^0$, given by

$$\langle \sigma v \rangle (\chi \bar{\chi} \rightarrow S^0 S^0) = \frac{3\lambda_{\chi S^0}^4}{64\pi m_\chi^2} \left(\frac{3}{x_f} \right) \theta(m_\chi - m_{S^0}) \quad (\text{C.7})$$

D Triple scalar coupling

Here, we extract the triple scalar coupling from the 2-HDM + singlet scalar Lagrangian in the alignment limit. Some of these scalars can be directly constrained from the ongoing experiments at the Colliders. We define dimensionless ratios $r_0 = \frac{m_{H^0}^2}{m_{h^0}^2}$ and $s_0 = \frac{m_{A^0}^2}{m_{h^0}^2}$. All triple scalar couplings are defined in terms of r_0 , s_0 and $\tan \beta$.

$$\begin{aligned} C_{h^0 S^0 S^0} &= \frac{\delta_{13}^2 m_{h^0}^2}{v_o} \left(-\frac{4\delta_{13}^2 r_0^2}{\tan \beta} + \frac{2\delta_{13}^2 r_0}{\tan \beta} - \frac{8r_0^3}{\tan^4 \beta} + \frac{8r_0^2 s_0}{\tan^3 \beta} + \frac{4r_0^2}{\tan^4 \beta} - \frac{8r_0 s_0}{\tan^3 \beta} - \frac{8r_0 s_0}{\tan \beta} \right. \\ &\quad \left. + \frac{2r_0}{\tan^4 \beta} - \frac{2r_0}{\tan^2 \beta} + \frac{2s_0}{\tan^3 \beta} + 2s_0 \tan \beta + \frac{4\delta_{13}^2 s_0}{\tan \beta} - \frac{1}{\tan^4 \beta} - \frac{2}{\tan^2 \beta} - 1 \right) \end{aligned} \quad (\text{D.1})$$

$$C_{S^0 h^0 h^0} = \frac{\delta_{13} m_{h^0}^2}{v_o} \left(-\frac{4\delta_{13}^2 r_0^2}{\tan^2 \beta} + \frac{2\delta_{13}^2 r_0}{\tan^2 \beta} - 2\delta_{13}^2 r_0 - \frac{6r_0}{\tan^3 \beta} - \frac{4r_0}{\tan \beta} \right) \quad (\text{D.2})$$

$$\begin{aligned} C_{S^0 H^0 H^0} &= \frac{\delta_{13} m_{h^0}^2}{v_o} \left(-\frac{8\delta_{13}^2 r_0^3}{\tan^2 \beta} + \frac{12\delta_{13}^2 r_0^2}{\tan^2 \beta} - \frac{4\delta_{13}^2 r_0}{\tan^2 \beta} - \frac{6r_0^2}{\tan^5 \beta} - \frac{4r_0^2}{\tan^3 \beta} + \frac{2r_0^2}{\tan \beta} + \frac{6r_0 s_0}{\tan^4 \beta} + \frac{4r_0 s_0}{\tan^2 \beta} \right. \\ &\quad \left. - 2r_0 s_0 + \frac{3r_0}{\tan^5 \beta} + \frac{r_0}{\tan^3 \beta} - 3r_0 \tan \beta - \frac{7r_0}{\tan \beta} - \frac{3s_0}{\tan^4 \beta} + 3s_0 \tan^2 \beta - \frac{3s_0}{\tan^2 \beta} + 3s_0 \right) \end{aligned} \quad (\text{D.3})$$

$$\begin{aligned} C_{S^0 S^0 H^0} &= \frac{\delta_{13}^2 m_{h^0}^2}{v_o} \left(-\frac{8\delta_{13}^2 r_0^3}{\tan^2 \beta} + \frac{8\delta_{13}^2 r_0^2}{\tan^2 \beta} - \frac{2\delta_{13}^2 r_0}{\tan^2 \beta} + \frac{12r_0^3}{\tan^5 \beta} + \frac{4r_0^3}{\tan^3 \beta} - \frac{12r_0^2 s_0}{\tan^4 \beta} - \frac{4r_0^2 s_0}{\tan^2 \beta} - \frac{12r_0^2}{\tan^5 \beta} \right. \\ &\quad \left. + \frac{8r_0^2}{\tan \beta} + \frac{12r_0 s_0}{\tan^4 \beta} + \frac{8r_0 s_0}{\tan^2 \beta} - 4r_0 s_0 + \frac{3r_0}{\tan^5 \beta} - \frac{r_0}{\tan^3 \beta} - 3r_0 \tan \beta - \frac{11r_0}{\tan \beta} \right. \\ &\quad \left. - \frac{3s_0}{\tan^4 \beta} + 3s_0 \tan^2 \beta - \frac{3s_0}{\tan^2 \beta} + 3s_0 \right) \end{aligned} \quad (\text{D.4})$$

$$C_{S^0 H^0 h^0} = \frac{\delta_{13} m_{h^0}^2}{v_o} \left(-\frac{4\delta_{13}^2 r_0^3}{\tan^3 \beta} + \frac{4\delta_{13}^2 r_0^2}{\tan^3 \beta} - \frac{4\delta_{13}^2 r_0^2}{\tan \beta} - \frac{\delta_{13}^2 r_0}{\tan^3 \beta} + \frac{3\delta_{13}^2 r_0}{\tan \beta} + \frac{4r_0^2}{\tan^4 \beta} + \frac{4r_0^2}{\tan^2 \beta} - \frac{4r_0 s_0}{\tan^3 \beta} - \frac{4r_0 s_0}{\tan \beta} - \frac{3r_0}{\tan^2 \beta} - r_0 + \frac{2s_0}{\tan^3 \beta} + 2s_0 \tan \beta + \frac{4s_0}{\tan \beta} - \frac{1}{\tan^4 \beta} - \frac{2}{\tan^2 \beta} - 1 \right) \quad (\text{D.5})$$

$$C_{S^0 H^+ H^-} = \frac{\delta_{13} m_{h^0}^2}{v_o} \left(-\frac{2r_0^2}{\tan^5 \beta} + \frac{2r_0^2}{\tan \beta} + \frac{2r_0 s_0}{\tan^4 \beta} + \frac{4r_0 s_0}{\tan^2 \beta} + 2r_0 s_0 + \frac{r_0}{\tan^5 \beta} - \frac{r_0}{\tan^3 \beta} - r_0 \tan \beta - \frac{5r_0}{\tan \beta} - \frac{s_0}{\tan^4 \beta} + s_0 \tan^2 \beta - \frac{s_0}{\tan^2 \beta} + s_0 - \frac{4m_{H^\pm}^2 r_0}{\tan^3 \beta m_{h^0}^2} - \frac{4m_{H^\pm}^2 r_0}{\tan \beta m_{h^0}^2} \right) \quad (\text{D.6})$$

$$C_{S^0 A^0 A^0} = \frac{\delta_{13} m_{h^0}^2}{v_o} \left(-\frac{4m_{A^0}^2 r_0}{\tan^3 \beta m_{h^0}^2} - \frac{4m_{A^0}^2 r_0}{\tan \beta m_{h^0}^2} - \frac{2r_0^2}{\tan^5 \beta} + \frac{2r_0^2}{\tan \beta} + \frac{2r_0 s_0}{\tan^4 \beta} + \frac{4r_0 s_0}{\tan^2 \beta} + 2r_0 s_0 + \frac{r_0}{\tan^5 \beta} - \frac{r_0}{\tan^3 \beta} - r_0 \tan \beta - \frac{5r_0}{\tan \beta} - \frac{s_0}{\tan^4 \beta} + s_0 \tan^2 \beta - \frac{s_0}{\tan^2 \beta} + s_0 \right) \quad (\text{D.7})$$

$$C_{S^0 S^0 S^0} = \frac{\delta_{13}^3 m_{h^0}^2}{v_o} \left(-\frac{24r_0^4}{\tan^5 \beta} + \frac{24r_0^3 s_0}{\tan^4 \beta} + \frac{36r_0^3}{\tan^5 \beta} - \frac{12r_0^3}{\tan^3 \beta} - \frac{36r_0^2 s_0}{\tan^4 \beta} - \frac{12r_0^2 s_0}{\tan^2 \beta} - \frac{18r_0^2}{\tan^5 \beta} + \frac{12r_0^2}{\tan^3 \beta} + \frac{18r_0 s_0}{\tan^4 \beta} + \frac{12r_0 s_0}{\tan^2 \beta} - 6r_0 s_0 + \frac{3r_0}{\tan^5 \beta} - \frac{3r_0}{\tan^3 \beta} - 3r_0 \tan \beta - \frac{15r_0}{\tan \beta} - \frac{3s_0}{\tan^4 \beta} + 3s_0 \tan^2 \beta - \frac{3s_0}{\tan^2 \beta} + 3s_0 \right) \quad (\text{D.8})$$

$$C_{h^0 H^+ H^-} = \frac{m_{h^0}^2}{v_o} \left(\frac{2\delta_{13}^2 r_0}{\tan \beta} + \frac{2s_0}{\tan^3 \beta} + 2s_0 \tan \beta + \frac{4s_0}{\tan \beta} - \frac{1}{\tan^4 \beta} - \frac{2}{\tan^2 \beta} - 1 - \frac{2m_{H^\pm}^2}{\tan^4 \beta m_{h^0}^2} - \frac{4m_{H^\pm}^2}{\tan^2 \beta m_{h^0}^2} - \frac{2m_{H^\pm}^2}{m_{h^0}^2} \right). \quad (\text{D.9})$$

References

- [1] M. Garny, A. Ibarra, M. Pato and S. Vogl, JCAP **1312**, 046 (2013) doi:10.1088/1475-7516/2013/12/046 [arXiv:1306.6342 [hep-ph]].
- [2] J. GoodMan, M. Ibe, A. Rajaraman, W. Shepherd, T. M. P. Tait and H. B. Yu, Phys. Lett. B **695**, 185 (2011) doi:10.1016/j.physletb.2010.11.009 [arXiv:1005.1286 [hep-ph]].
- [3] J. Hisano, K. Ishiwata and N. Nagata, Phys. Lett. B **706**, 208 (2011) doi:10.1016/j.physletb.2011.11.017 [arXiv:1110.3719 [hep-ph]].
- [4] M. Garny, A. Ibarra, M. Pato and S. Vogl, JCAP **1211**, 017 (2012) doi:10.1088/1475-7516/2012/11/017 [arXiv:1207.1431 [hep-ph]].
- [5] M. Ackermann *et al.* [Fermi-LAT Collaboration], Phys. Rev. D **89**, 042001 (2014) doi:10.1103/PhysRevD.89.042001 [arXiv:1310.0828 [astro-ph.HE]].
- [6] C. Y. Chen, H. Davoudiasl, W. J. Marciano and C. Zhang, Phys. Rev. D **93**, no. 3, 035006 (2016) doi:10.1103/PhysRevD.93.035006 [arXiv:1511.04715 [hep-ph]].
- [7] PDG 2018 review rpp2018-rev-g-2-muon-anom-mag-moment.pdf

- [8] K. Hagiwara, R. Liao, A. D. Martin, D. Nomura and T. Teubner, *J. Phys. G* **38**, 085003 (2011) doi:10.1088/0954-3899/38/8/085003 [arXiv:1105.3149 [hep-ph]].
- [9] PDG 2018 review rpp2018-list-electron.pdf
- [10] B. Batell, N. Lange, D. McKeen, M. Pospelov and A. Ritz, *Phys. Rev. D* **95**, no. 7, 075003 (2017) doi:10.1103/PhysRevD.95.075003 [arXiv:1606.04943 [hep-ph]].
- [11] C. Bird, P. Jackson, R. V. Kowalewski and M. Pospelov, *Phys. Rev. Lett.* **93**, 201803 (2004) doi:10.1103/PhysRevLett.93.201803 [hep-ph/0401195].
- [12] D. O'Connell, M. J. Ramsey-Musolf and M. B. Wise, *Phys. Rev. D* **75**, 037701 (2007) doi:10.1103/PhysRevD.75.037701 [hep-ph/0611014].
- [13] B. Batell, M. Pospelov and A. Ritz, *Phys. Rev. D* **83**, 054005 (2011) doi:10.1103/PhysRevD.83.054005 [arXiv:0911.4938 [hep-ph]].
- [14] G. Krnjaic, *Phys. Rev. D* **94**, no. 7, 073009 (2016) doi:10.1103/PhysRevD.94.073009 [arXiv:1512.04119 [hep-ph]].
- [15] J. P. Lees *et al.* [BaBar Collaboration], *Phys. Rev. D* **94**, no. 1, 011102 (2016) doi:10.1103/PhysRevD.94.011102 [arXiv:1606.03501 [hep-ex]].
- [16] M. Battaglieri *et al.*, *Nucl. Instrum. Meth. A* **777**, 91 (2015) doi:10.1016/j.nima.2014.12.017 [arXiv:1406.6115 [physics.ins-det]].
- [17] O. Lebedev, W. Loinaz and T. Takeuchi, *Phys. Rev. D* **62**, 055014 (2000) doi:10.1103/PhysRevD.62.055014 [hep-ph/0002106].
- [18] P. Agrawal, Z. Chacko and C. B. Verhaaren, *JHEP* **1408**, 147 (2014) doi:10.1007/JHEP08(2014)147 [arXiv:1402.7369 [hep-ph]].
- [19] S. Schael *et al.* [ALEPH and DELPHI and L3 and OPAL and LEP Electroweak Collaborations], *Phys. Rept.* **532**, 119 (2013) doi:10.1016/j.physrep.2013.07.004 [arXiv:1302.3415 [hep-ex]].
- [20] G. Aad *et al.* [ATLAS Collaboration], *JHEP* **1603**, 127 (2016) doi:10.1007/JHEP03(2016)127 [arXiv:1512.03704 [hep-ex]].
- [21] V. Ilisie, *JHEP* **1504**, 077 (2015) doi:10.1007/JHEP04(2015)077 [arXiv:1502.04199 [hep-ph]].
- [22] J. Abdallah *et al.* [DELPHI Collaboration], *Eur. Phys. J. C* **38**, 1 (2004) doi:10.1140/epjc/s2004-02011-4 [hep-ex/0410017].b
- [23] PDG 2018 review rpp2018-rev-higgs-muon-boson.pdf
- [24] ATLAS NOTE ATL-PHYS-PUB-2016-024, The ATLAS Collaboration, (2016).
- [25] P. A. R. Ade *et al.* [Planck Collaboration], *Astron. Astrophys.* **594**, A13 (2016) doi:10.1051/0004-6361/201525830 [arXiv:1502.01589 [astro-ph.CO]].
- [26] E. Komatsu *et al.* [WMAP Science Team], *PTEP* **2014**, 06B102 (2014) doi:10.1093/ptep/ptu083 [arXiv:1404.5415 [astro-ph.CO]].
- [27] F. Tanedo, Defense against the Dark Arts, <http://www.physics.uci.edu/tanedo/files/notes/DMNotes.pdf>
- [28] F. Ambrogio, C. Arina, M. Backovic, J. Heisig, F. Maltoni, L. Mantani, O. Mattelaer and G. Mohlabeng, arXiv:1804.00044 [hep-ph].

- [29] J. Alwall, M. Herquet, F. Maltoni, O. Mattelaer and T. Stelzer, JHEP **1106**, 128 (2011) doi:10.1007/JHEP06(2011)128 [arXiv:1106.0522 [hep-ph]].
- [30] A. Alloul, N. D. Christensen, C. Degrande, C. Duhr and B. Fuks, Comput. Phys. Commun. **185**, 2250 (2014) doi:10.1016/j.cpc.2014.04.012 [arXiv:1310.1921 [hep-ph]].
- [31] G. Bhattacharyya and D. Das, Pramana **87**, no. 3, 40 (2016) doi:10.1007/s12043-016-1252-4 [arXiv:1507.06424 [hep-ph]].
- [32] A. Broggio, E. J. Chun, M. Passera, K. M. Patel and S. K. Vempati, JHEP **1411**, 058 (2014) doi:10.1007/JHEP11(2014)058 [arXiv:1409.3199 [hep-ph]].
- [33] J. Kopp, V. Niro, T. Schwetz and J. Zupan, Phys. Rev. D **80**, 083502 (2009) doi:10.1103/PhysRevD.80.083502 [arXiv:0907.3159 [hep-ph]].
- [34] J. Kopp, L. Michaels and J. Smirnov, JCAP **1404**, 022 (2014) doi:10.1088/1475-7516/2014/04/022 [arXiv:1401.6457 [hep-ph]].
- [35] F. D’Eramo, B. J. Kavanagh and P. Panci, Phys. Lett. B **771**, 339 (2017) doi:10.1016/j.physletb.2017.05.063 [arXiv:1702.00016 [hep-ph]].
- [36] X. Cui *et al.* [PandaX-II Collaboration], Phys. Rev. Lett. **119**, no. 18, 181302 (2017) doi:10.1103/PhysRevLett.119.181302 [arXiv:1708.06917 [astro-ph.CO]].
- [37] E. Aprile *et al.* [XENON Collaboration], JCAP **1604**, no. 04, 027 (2016) doi:10.1088/1475-7516/2016/04/027 [arXiv:1512.07501 [physics.ins-det]].
- [38] E. Aprile *et al.* [XENON Collaboration], Eur. Phys. J. C **77**, no. 12, 881 (2017) doi:10.1140/epjc/s10052-017-5326-3 [arXiv:1708.07051 [astro-ph.IM]].
- [39] M. Ackermann *et al.* [Fermi-LAT Collaboration], Phys. Rev. Lett. **115**, no. 23, 231301 (2015) doi:10.1103/PhysRevLett.115.231301 [arXiv:1503.02641 [astro-ph.HE]].
- [40] M. Ajello *et al.* [Fermi-LAT Collaboration], Astrophys. J. **819**, no. 1, 44 (2016) doi:10.3847/0004-637X/819/1/44 [arXiv:1511.02938 [astro-ph.HE]].
- [41] S. Profumo, F. S. Queiroz, J. Silk and C. Siqueira, JCAP **1803**, no. 03, 010 (2018) doi:10.1088/1475-7516/2018/03/010 [arXiv:1711.03133 [hep-ph]].
- [42] M. Lisanti, L. E. Strigari, J. G. Wacker and R. H. Wechsler, Phys. Rev. D **83**, 023519 (2011) doi:10.1103/PhysRevD.83.023519 [arXiv:1010.4300 [astro-ph.CO]].
- [43] V. Khachatryan *et al.* [CMS Collaboration], Phys. Rev. D **90**, 112013 (2014) doi:10.1103/PhysRevD.90.112013 [arXiv:1410.2751 [hep-ex]].
- [44] D. Chowdhury and O. Eberhardt, arXiv:1711.02095 [hep-ph].